

## FEDSM-ICNMM2010-30071

### VIBRO-IMPACT EXPERIMENTS AND COMPUTATIONS OF A GAP-SUPPORTED TUBE SUBJECTED TO SINGLE-PHASE FLUID-ELASTIC COUPLING FORCES

**Philippe Piteau**

Commissariat à l'Énergie Atomique  
Laboratoire d'Études de Dynamique  
CEA,DEN,DM2S,SEMT,DYN  
Saclay, France

**Xavier Delaune**

Commissariat à l'Énergie Atomique  
Laboratoire d'Études de Dynamique  
CEA,DEN,DM2S,SEMT,DYN  
Saclay, France

**Jose Antunes**

Instituto Tecnológico e Nuclear  
Applied Dynamics Laboratory  
ITN,ADL  
Sacavem, Portugal

**Laurent Borsoi**

Commissariat à l'Énergie Atomique  
Laboratoire d'Études de Dynamique  
CEA,DEN,DM2S,SEMT,DYN  
Saclay, France

#### ABSTRACT

In this paper we address the problem of computing the nonlinear vibro-impact responses of gap-supported heat-exchanger tubes subjected to fluid-elastic coupling forces, as well as to the turbulence excitation from transverse flows. Emphasis is on the fluid-elastic modeling within a time-domain nonlinear framework, as well as on the stabilizing effect of impacts on the fluid-elastic coupling forces.

Theoretical computations of the linear and vibro-impacting regimes of a flow-excited cantilever test tube, within a rigid  $3 \times 5$  square bundle, are based on the experimentally identified fluid-elastic coupling force coefficients and turbulence spectrum. Computations are then compared with the experimental vibratory responses, enabling a full validation of the modeling approach. Furthermore, interesting conclusions are drawn, concerning: (a) the energy balance between sources and sinks, for a vibro-impacting tube subjected to fluid-elastic forces; (b) the dependence of the vibration response frequency on impacts at the loose supports, and their effect on the nonlinear re-stabilization of fluid-elastically unstable tubes.

Details on the following aspects are reported in the paper: (1) Numerical modeling of the fluid-elastic coupling forces for time-domain computations; (2) Experimental identification of the fluid-elastic coupling coefficients; (3) Computations and

experiments of both linear and vibro-impacting responses under the combined action of turbulence and fluid-elastic coupling; and (4) Energy aspects of the vibro-impacting fluid-elastically coupled tube responses.

#### NOMENCLATURE

$A$	Area of the tube cross-section
$C_d$	Dimensionless damping coupling coefficient
$C_k$	Dimensionless stiffness coupling coefficient
$C_m$	Dimensionless inertia coupling coefficient
$[\mathcal{D}_s]$	Structural modal damping matrix
$[\mathcal{D}_F(t)]$	Fluid-elastic modal damping matrix
$D$	Tube diameter
$D_F$	Fluid-elastic damping coupling coefficient
$E$	Young's modulus of the tube
$f$	Frequency
$\bar{f}_r$	Response frequency estimate
$f_R = \bar{f}_r D/V$	Reduced frequency
$f(x,t)$	Total excitation force field
$f_F(x,t)$	Fluid-elastic coupling force field

$f_T(x, t)$	Turbulence force field
$f_C(x, t)$	Contact/impact force field
$F_C(t)$	Contact/impact force at support $x_C$
$F_n(t)$	Total modal force (mode $n$ )
$F_n^F(t)$	Fluid-elastic component of the modal force
$F_n^T(t)$	Turbulence component of the modal force
$F_n^C(t)$	Contact/impact component of the modal force
$\{\mathcal{F}(t)\}$	Vector of modal forces
$I$	Moment of inertia of the tube cross-section
$K_F$	Fluid-elastic stiffness coupling coefficient
$K_C$	Tube/support contact stiffness
$[\mathcal{K}_S]$	Structural modal stiffness matrix
$[\mathcal{K}_F(t)]$	Fluid-elastic modal stiffness matrix
$L$	Tube length
$M_F$	Fluid-elastic inertia coupling coefficient
$m_n$	Modal masse (mode $n$ )
$[\mathcal{M}_S]$	Structural modal mass matrix
$[\mathcal{M}_F]$	Fluid-elastic modal mass matrix
$n = 1, 2, \dots, N$	Modal index
$q_n(t)$	Modal response (mode $n$ )
$\{Q(t)\}$	Vector of modal amplitudes
$t$	Time
$T$	Total simulation duration
$V$	Transverse inter-tubes flow velocity
$V_R = V/\bar{f}_r D$	Reduced velocity
$x$	Location along the tube
$Y(x, t)$	Flexural tube response
$\delta_c$	Support gap
$\rho$	Mass density of the tube
$\eta$	Tube viscous dissipation coefficient
$\sigma$	RMS value of the tube displacement
$\omega_n$	Modal circular frequency (mode $n$ )
$\zeta_n$	Modal damping (mode $n$ )
$\varphi_n(x)$	Modeshape (mode $n$ )
$[\Phi]_e(f_R)$	Dimensionless equivalent spectrum

## 1. INTRODUCTION

It is well known that heat-exchanger tube bundles are subjected to fluid-elastic coupling forces, which depend on the bundle geometry, fluid nature (single-phase or two-phase) and on the fluid velocity. Reliable modeling of such coupling forces is very difficult, therefore several authors since the pioneering work of Tanaka & Takahara [1] have attempted to measure the fluid-elastic linearized stiffness and damping coefficients as a

function of the flow reduced velocity (or reduced frequency), for specific fluid mixtures and bundle geometries, in order to link the dynamical behavior of the flow-coupled tube bundle with simpler stability criteria such as provided by Connors [2] and many others since.

When looking at the gap-supported tubes of real-life components, time-domain nonlinear computing methods have been developed by several research groups for the predictive analysis of vibro-impacting flow-excited tubes. As far as fluid-elastic forces are concerned, the first attempt to include them in the computations – along with the ever-present turbulent excitation – was achieved by Axisa et al. [3], who used a flow velocity-dependent negative damping coefficient on the linearly unstable mode, deduced from Connors formulation. This pioneering approach was followed by others, along similar lines – see Fricker [4], for instance, who additionally corrected the computation of the fluid-elastic coupling effect by using an estimate of the actual response frequency instead of the modal frequency of the unstable mode. Since then, others have tackled this problem in a more sophisticated manner, by directly incorporating in their computer programs models of the fluid-elastic coupling forces [5-8].

Nevertheless, it is still debatable how realistic are the strongly nonlinear and unsteady vibro-impact regimes produced by computations which stem from fluid-elastic coefficients obtained under linear and steady (harmonic) conditions. Furthermore, it is well known that, when gap-supported tubes become linearly unstable, impacting produces an increase of the actual tube response frequencies, which somehow tend to re-stabilize the system. Because of these difficulties, there is urgency in confronting the rationale of such computational approach with actual experimental results. Such is the aim of the present paper. Vibro-impact controlled experiments under linearly unstable conditions were performed in the past by Antunes et al. [9] and Vento et al. [10]. However, in their work, the tube instability was created by an electro-mechanical feedback-controlled system, such that the “fluid-elastic” coupling stiffness coefficient was nil and the coupling damping coefficient was independent of the system response frequency. A different exploratory angle has been investigated by Mureithi et al. [11], who performed fractal-dimension computations on pseudo-phase space reconstructions from the flow-induced responses of a multi-supported tube, in order to distinguish the (post-Hopf bifurcation) fluid-elastically unstable chaotic vibro-impact responses from the randomness due to turbulence. Although all these former experiments produced interesting qualitative results, in the case of real flow-excited tube bundles, these are unrealistic over-simplifications. We believe that carefully controlled experiments of gap supported tubes subjected to fluid-elastic coupling forces are needed, in view of validating the current computational approaches for such systems, as well as to increase our physical understanding of the stabilizing mechanisms provided by the impact dynamics.

Therefore, based on the active vibration control method proposed by Caillaud et al. [12-14], new experiments have

recently been performed at CEA-Saclay on the same experimental rig, consisting on a flexible tube (vibrating along the lift direction) inserted in a rigid square bundle. First, the linearized fluid-elastic coupling coefficients, as well as the turbulence excitation, were identified for a significant range of reduced velocity, in water cross-flow. Then, nonlinear experiments were performed under the same conditions after installing an instrumented loose support in the rig, from which both the tube responses and the impact forces were measured.

These experimental results are compared with the linear and vibro-impact numerically simulated responses obtained from a time-domain computer program, where the experimentally identified linear fluid-elastic coupling coefficients were implemented. A delicate aspect of such implementation is the real-time estimation of a representative instantaneous response frequency of the vibro-impacting tube, which is needed because the coupling coefficients depend on the “instantaneous” reduced frequency. We mention several techniques for such frequency tracking, and propose a new one for near-“real-time” estimation of the nonlinear tube response frequency. Then a satisfying comparison between the experimental results and nonlinear computed predictions is produced, which validates our current computational approach for linearly unstable gap-supported tubes. On the other hand, computations show the energy aspects behind the nonlinear stabilization of fluid-elastically unstable tubes, as well as their relation with the increase in the tube response frequency due to impacts.

## 2. NUMERICAL MODELING OF THE FLOW-EXCITED GAP-SUPPORTED TUBE

### 2.1. Time-Domain Computation of the Nonlinear Dynamics

As discussed in [3,15], the simple Bernoulli–Euler theory for flexural vibrations proved to be adequate for impact identification. Therefore, assuming a viscous damping model, the small-amplitude flexural response of a tube with constant cross-sectional properties is described by the differential equation:

$$\rho A \frac{\partial^2 Y}{\partial t^2} + \eta \frac{\partial Y}{\partial t} + EI \frac{\partial^4 Y}{\partial x^4} = f(x,t) = f_F(x,t) + f_T(x,t) + f_C(x,t) \quad (1)$$

where  $f(x,t)$  is the total external excitation field and  $Y(x,t)$  is the tube transverse flexural response,  $E$  is Young’s modulus and  $\rho$  is the mass density of the tube,  $A$  is the area and  $I$  is the moment of inertia of the cross-section, while  $\eta$  is a viscous dissipation coefficient. The total excitation field in equation (1) stems from the fluid-elastic coupling forces  $f_F(x,t)$ , the turbulence forces  $f_T(x,t)$  and the contact/impact forces  $f_C(x,t) = \sum_C F_C(t) \delta(x - x_C)$  located at the loose supports  $x_C$ .

As amply discussed by Axisa et al. [3] and Antunes et al. [16], the vibro-impact nonlinear computations under flow excitation may be performed in an effective manner by

projecting equation (1) on the tube unconstrained modes  $\varphi_n(x)$ . Then, the following discretized modal equations are obtained:

$$m_n \ddot{q}_n + 2m_n \omega_n \zeta_n \dot{q}_n + m_n \omega_n^2 q_n = F_n(t) = F_n^F(t) + F_n^T(t) + F_n^C(t) \quad (2)$$

in terms of the modal amplitudes  $q_n(t)$  and its derivatives, with the modal masses  $m_n$ , frequencies  $\omega_n$  and damping values  $\zeta_n$ ,  $n = 1, 2, \dots, N$ . In matrix notation:

$$[\mathcal{M}_s] \{\ddot{Q}\} + [\mathcal{D}_s] \{\dot{Q}\} + [\mathcal{K}_s] \{Q\} = \{\mathcal{F}^F(t)\} + \{\mathcal{F}^T(t)\} + \{\mathcal{F}^C(t)\} \quad (3)$$

The total modal forces  $F_n(t)$  in the right hand side of equation (2) are computed from the modal projections of the fluid-elastic, turbulence and contact/impact terms :

$$F_n^F(t) = \int_0^L f_F(x,t) \varphi_n(x) dx \quad ; \quad F_n^T(t) = \int_0^L f_T(x,t) \varphi_n(x) dx \quad (4)$$

$$F_n^C(t) = \int_0^L \left( \sum_C F_C(t) \delta(x - x_C) \right) \varphi_n(x) dx = \sum_C F_C(t) \varphi_n(x_C)$$

where  $L$  is the tube length.

The physical motions may be computed from the modal responses at any time and location, by modal superposition:

$$Y(x,t) = \sum_{n=1}^N \varphi_n(x) q_n(t) \quad (5)$$

and similarly for all time-derivatives. The computational truncation index  $N$  of the modal basis is chosen accounting for the frequency ranges excited by the various sources of excitation.

### 2.2. Fluid-elastic Coupling Forces

In their recent work, Hassan & Hayder [8] developed a direct implementation of the Lever and Weaver [17] model to compute the fluid-elastic coupling forces, which does not require the knowledge of the instantaneous tube response frequency. However, the most common approach – and the only available if one wishes to use experimentally identified force data – is to express the linearized fluid-elastic forces  $f_F(x,t)$  in terms of coupling coefficients  $M_F$ ,  $D_F$  and  $K_F$ , which in general depend on  $V_R$ . Then, the fluid-elastic force reads:

$$f_F(x,t) = -M_F \ddot{Y}(x,t) - D_F(V_R(x,t)) \dot{Y}(x,t) - K_F(V_R(x,t)) Y(x,t) \quad (6)$$

where only the fluid inertia coupling coefficient does not depend on the reduced flow velocity  $V_R(x,t)$ , here defined as:

$$V_R(x,t) = V(x) \left[ \bar{f}_r(x,t) D \right] \quad (7)$$

with  $\bar{f}_r(x,t)$  an estimate of the “instantaneous” local response frequency of the nonlinearly vibrating tube. It is convenient to define dimensionless coupling coefficients, which may be presented in the following form [1,18]:

$$C_m = \frac{M_F}{(1/2) \rho D^2 L} \quad ; \quad C_d(V_R) = \frac{D_F(V_R)}{(1/2) \rho D V L} \quad ; \quad C_k(V_R) = \frac{K_F(V_R)}{(1/2) \rho V^2 L} \quad (8)$$

Then, after modal projections, the fluid-elastic force field (6) leads to the following modal forces:

$$\{\mathcal{F}^F(t)\} = -[\mathcal{M}_F]\{\ddot{Q}\} - [\mathcal{D}_F(t)]\{\dot{Q}\} - [\mathcal{K}_F(t)]\{Q\} \quad (9)$$

where the terms of the modal fluid-elastic coupling matrices are computed as:

$$\begin{aligned} m_{nm}^F &= \int_0^L M_F \varphi_n(x) \varphi_m(x) dx \\ d_{nm}^F(t) &= \int_0^L D_F(V_R(x,t)) \varphi_n(x) \varphi_m(x) dx \\ k_{nm}^F(t) &= \int_0^L K_F(V_R(x,t)) \varphi_n(x) \varphi_m(x) dx \end{aligned} \quad (10)$$

From (3) and (9) one can obtain the changes in the system modal properties, due to the fluid-elastic coupling, as a function of the flow velocity. In the frequency domain:

$$\left[ \lambda^2([\mathcal{M}_S] + [\mathcal{M}_F]) + \lambda([\mathcal{D}_S] + [\mathcal{D}_F(V_R)]) + ([\mathcal{K}_S] + [\mathcal{K}_F(V_R)]) \right] \{\bar{Q}\} = \{0\} \quad (11)$$

where  $\lambda_n(V_R) = \sigma_n(V_R) \pm i\nu_n(V_R)$  are the complex eigenvalues of the flow-coupled system, which are related to the modal properties as:

$$\omega_n(V_R) = \sqrt{\sigma_n^2(V_R) + \nu_n^2(V_R)} \quad ; \quad \zeta_n(V_R) = -\sigma_n(V_R) / \omega_n(V_R) \quad (12)$$

Notice that, because the modal coupling coefficients depend on the response frequencies encapsulated in  $V_R$ , the eigen-computation (11) should be performed in iterative manner.

### 2.3. Turbulence Forces

Modeling of the turbulence excitation  $f_T(x,t)$  by the transverse flow is based on the general theory developed by Axisa et al. [19]. Then, generation of time-domain realizations of the turbulence forces is achieved using the efficient method recently proposed by Antunes et al. [20-21].

Accordingly, we start from the measured equivalent reference spectrum  $[\Phi]_e(f_r)$  of the turbulence forces per unit tube length, where  $f_r = \bar{f}_r D / V$  is the reduced frequency. Then, a set of uncorrelated random point forces is applied along the tube, using a computation technique which preserves the spectral content as well as the space correlation of the original turbulence force field, accounting for the flow velocity profile. See the aforementioned references for details.

### 2.4. Contact Forces at Loose Supports

A single nonlinear loose support is assumed in this paper, in accordance with the experimental rig. The contact force  $F_C(t)$  is computed in an explicit manner from the system response, at each time-step, using the following penalty formulation:

$$F_C(t) = \begin{cases} -K_C [Y(x_c, t) - \delta_C] & \text{if } |Y(x_c, t)| > |\delta_C| \\ 0 & \text{if } |Y(x_c, t)| < |\delta_C| \end{cases} \quad (13)$$

where  $K_C$  is a suitable value for the contact stiffness at the support, which is pragmatically adjusted such that the numerical simulations reproduce the elementary contact duration of the experimental impacts. Because the tube motions studied in this

paper are planar and the corresponding impacts only display a radial component, there is no need to implement a friction contact model [16].

One may notice, from equations (5) and (13), that the tube/support interaction couples the system unconstrained modes. Indeed, during contact, one obtains:

$$F_C(t) = -K_C \left[ \sum_{n=1}^N \varphi_n(x_c) q_n(t) - \delta_C \right] \quad (14)$$

which clearly shows that the tube/support impacts couple all modes, redistributing the modal energies.

### 2.5. Quasi-Instantaneous Response Frequency

As stated earlier, an estimate of some representative ‘‘instantaneous’’ response frequency  $\bar{f}_r(x,t)$  of the impacting tube is needed when performing time-domain numerical simulations, because the fluid-elastic coefficients depend on the reduced velocity  $V_R(x,t)$ . Several methods have been used by researchers in this field, including straight time-domain evaluations of the zero-crossing frequency or a time-window adaptation of Rice’s formula [22]:

$$\bar{f}_r(x,t) = \frac{1}{2\pi} \frac{\sigma_{\dot{y}}(x,t;\tau)}{\sigma_y(x,t;\tau)} \quad (15)$$

where  $\sigma_y(x,t;\tau)$  is the RMS value of the vibratory displacement at location  $x$ , computed within the updated time-window of size  $\tau$ , e.g.  $[t - \tau, t]$ , and  $\sigma_{\dot{y}}(x,t;\tau)$  is the RMS value of the corresponding velocity. An equivalent measure may be defined in the frequency domain, the spectra pertaining to the signal time-windowed within  $\tau$  [23]:

$$\bar{f}_r(x,t) = \int_0^{f_{\max}} f^2 S_{YY}(x,f;\tau) df / \int_0^{f_{\max}} S_{YY}(x,f;\tau) df \quad (16)$$

Other methods can be adapted from various fields involving non-stationary signals, for instance in voice and music analysis, where several time-domain and frequency-domain techniques are used for the frequency (pitch) tracking in speech and singing, including auto-correlation, auto-regressive, maximum likelihood, adaptive filtering and cepstral techniques – see [24,25] for reviews. Even so, for the computations of the present study, we have developed a simple estimation method which proved to be efficient and reliable enough. It is based on a least-squares fit of the parameters of an ‘‘equivalent’’ 1-dof oscillator, to the nonlinear computed responses within the sliding time window  $\tau$ :

$$\begin{Bmatrix} \ddot{Y}(x,t) \\ \vdots \\ \dot{Y}(x,t-\tau) \end{Bmatrix} + A \begin{Bmatrix} \dot{Y}(x,t) \\ \vdots \\ \dot{Y}(x,t-\tau) \end{Bmatrix} + B \begin{Bmatrix} Y(x,t) \\ \vdots \\ Y(x,t-\tau) \end{Bmatrix} = \begin{Bmatrix} 0 \\ \vdots \\ 0 \end{Bmatrix} \quad (17)$$

hence:

$$\begin{Bmatrix} A \\ B \end{Bmatrix} = - \left[ \begin{Bmatrix} \dot{Y}(x,t) \\ \vdots \\ \dot{Y}(x,t-\tau) \end{Bmatrix}, \begin{Bmatrix} Y(x,t) \\ \vdots \\ Y(x,t-\tau) \end{Bmatrix} \right]^+ \begin{Bmatrix} \ddot{Y}(x,t) \\ \vdots \\ \ddot{Y}(x,t-\tau) \end{Bmatrix} \quad (18)$$

where (+) stands for the pseudo-inversion of the rectangular

time-discretized matrix  $[\{\dot{Y}\}, \{Y\}]$ . Then, the equivalent frequency and damping parameters of the 1-dof fit to the nonlinear data are:

$$\bar{f}_r = \sqrt{B}/(2\pi) \quad ; \quad \bar{\zeta}_r = A/(4\pi\bar{f}_r) \quad (19)$$

All the discussed methods introduce a short-time delay, of order  $\tau/2$ , in the frequency estimate. The choice of  $\tau$  is a tradeoff between the reliability of the frequency estimate and the tolerated latency. For the purpose of the present study, a value of the order  $\tau \sim 1/f_1$  was found adequate. Also note – and this is a point often overlooked or insufficiently stressed in the literature – that the “instantaneous” response frequency of the nonlinearly vibrating tube is actually a *local* property. For multi-supported tubes, irrespectively of the technique used to estimate  $\bar{f}_r(x,t)$ , response frequencies computed near the loose supports are significantly higher than near mid-spans. This is because, near  $x_c$ , the vibratory responses are dominated by a local rattling behavior of the tube, meaning that the contribution of higher-order modes is comparatively much higher there than near mid-spans. Therefore, except for very short tubes, one should not use a single value of  $\langle \bar{f}_r(t) \rangle$  for the complete system, but compute  $\bar{f}_r(x,t)$  along the tube. This leads to different reduced velocities  $V_R(x,t)$ , hence different coefficients  $D_F(V_R(x,t))$  and  $K_F(V_R(x,t))$  along the tube, which are then properly weighted according to equations (10).

## 2.6. Numerical Simulations of the Gap-Supported Tube

The method described in the previous section was used to simulate the nonlinear dynamical responses of a clamped-free flexible test tube, within a rigid square bundle, which is excited by the turbulence of a uniform transverse flow and subjected to fluid-elastic coupling. The modeled tube has a length subjected to cross-flow  $L_f = 300$  mm and external diameter  $D = 30$  mm. At half-length, a loose support is modeled using two opposite springs with stiffnesses  $K_C = 10^6$  N/m, this value having been adjusted in order to reproduce the experimental elemental tube/support spike contact time ( $t_c = 2 \times 10^{-3}$  sec). As a result of the clamping fixture, the tube motions are constrained to be planar, along the lift direction. Three different support configurations have been simulated: (a) with no loose support (for linear responses); (b) with a symmetrical loose support  $\delta_C = \pm 0.5$  mm, and (c) with  $\delta_C = \pm 1$  mm. Because the test tube is quite short ( $L/D = 10$ ), the main contribution for the vibratory responses is from the first mode. Therefore, in the specific case of our experiments, the dominant response frequency is mostly the same irrespectively of the tube coordinate, hence  $\langle \bar{f}_r(t) \rangle \approx \bar{f}_r(x,t), \forall x$ . Ten modes, with frequencies in the range  $f_n \approx 18$  Hz  $\sim$  10 kHz (in stagnant

water) were used for the nonlinear computations. Numerical integration of the nonlinear formulation (3)-(14) is achieved using an explicit method, based on the analytical solution of the modal equations in state-space (first-order) form, with constant acceleration assumed within the time-step (Hart & Wong, 1999). Simulations were performed for a total time of 40 seconds. An illustrative typical result obtained from the previously described techniques is shown in Fig. 1. Notice how, as expected, the estimate of the “instantaneous” frequency  $\langle \bar{f}_r(t) \rangle$ , computed from (18)-(19), increases significantly when the tube impacts.

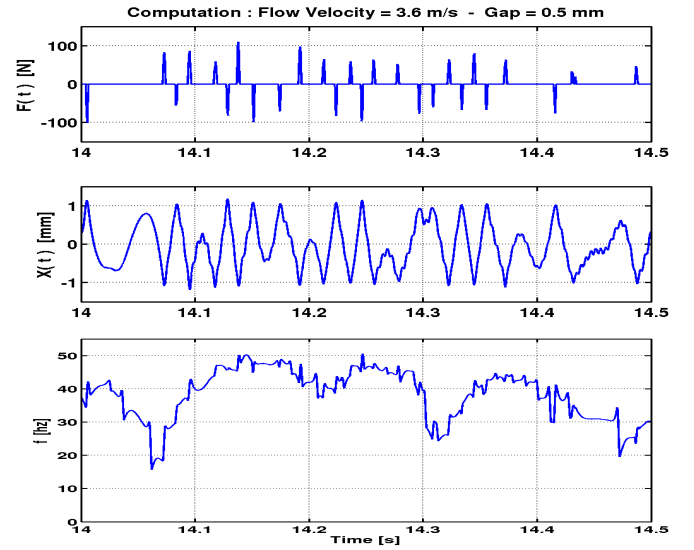


Figure 1: Illustrative vibro-impact computation and estimate of the “instantaneous” response frequency

## 3. EXPERIMENTAL RIG AND TEST PROCEDURES

The test rig is shown in Figs. 2 and 3. It is, essentially, the one used in [12-14] in their tests, however a new instrumented tube with quite different modal frequency was used in the present experiments. Furthermore, the present experiments were designed for flow-excited vibro-impacting on an instrumented loose support. The flexible steel tube, with the previously stated length  $L_f$  and diameter  $D$ , has a thin wall  $e = 0.5$  mm, being relatively light when compared with the added mass from the external fluid. The tube is clamped through a flat bar of length 100 mm, in order to constrain the vibrations to be planar. This tube is the central one of a  $3 \times 5$  square bundle of rigid tubes with reduced pitch  $P/D = 1.5$  (plus two columns of 5 half-tubes at the boundaries). The first modal frequency of the rigid tubes lay beyond 1 kHz, two orders of magnitude higher than the first modal frequency of the flexible tube.

A single-phase water flow is imposed along the vertical direction, with inter-tubes velocity in the range  $V = 0 \sim 4$  m/s. Measurement of the tube dynamical displacement, along the lift (horizontal) direction, was provided by a Zimmer camera OHG-

100A, pointed toward the end of the tube. As shown in Fig. 1, for the nonlinear tests, two instrumented gap-stops were located symmetrically at the tube half-length. The impact force measurements were performed by two piezoelectric force transducers Kistler 9132A.

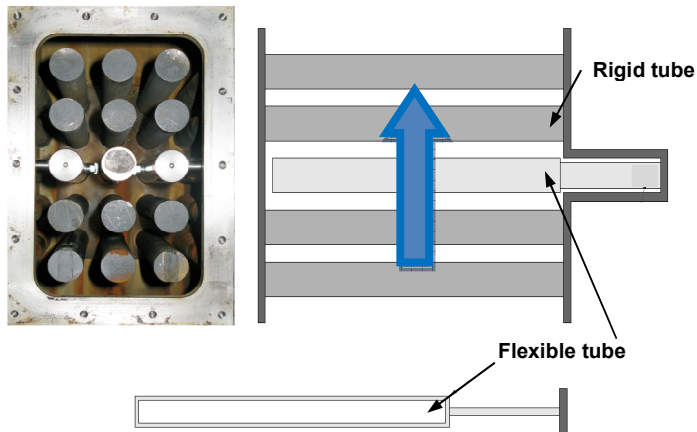


Figure 2: Experimental rig



Figure 3: Electromagnetic shaker for feedback control of the tube damping and stabilization

The first tests, performed under linear conditions (no loose support), were intended for the experimental identification of the fluid-elastic coupling coefficients  $C_d(V_R)$  and  $C_k(V_R)$ , the added mass  $C_m$  being assumed independent of the flow velocity. In order to explore the full range of experimental reduced velocity – well beyond the fluid-elastic stability boundary of the “normal” system – the analog feedback stabilization technique [12-14] has been adopted. It is, essentially, the one used earlier by Antunes et al. [9] in their feedback controlled instability tests, but with reversed polarity. As implemented in the present experiments at CEA, the flexible tube was fitted with an accelerometer Endevco 2222C, located near the node of the tube second mode, whose response signal was electronically time-integrated and amplified, being then fed to the electromechanical shaker shown in Fig. 3. A negative feedback loop was thus created, enabling a higher value of the tube first mode damping, which was controlled through the gain

of the power amplifier. Note that, due to the filtering used in the feedback loop to avoid undue modal spillover, the control force was not exactly in phase with the tube velocity. As a result, some residual feedback also affected the stiffness term, resulting in a change of the controlled tube modal frequency. This effect was carefully corrected when extracting the flow-coupling coefficients from the identified modal parameters.

This control system enabled us to identify the fluid-elastic coefficients in the range  $V = 0 \sim 2.5$  m/s, corresponding to a reduced velocity of about  $V_R = 0 \sim 5$ , beyond which even the feedback loop was unable to cope with the fluid-elastic destabilizing forces. However, for the vibro-impact tests, the full velocity range  $V = 0 \sim 4$  m/s was explored.

#### 4. FLUIDELASTIC AND TURBULENCE FORCES FROM THE TRANSVERSE FLOW

##### 4.1. Identified Fluid-Elastic Force Coefficients

Because the added mass  $C_m$  is assumed independent of the flow velocity, the inertia coupling by the flow is trivially obtained by comparing the modal frequencies in air and in stagnant fluid, respectively 31 Hz and 18 Hz for the first mode. Similarly, the viscous fluid damping coefficient  $C_d(0)$  at zero velocity can be inferred from the modal damping values in air and in stagnant fluid, respectively 0.33 % and 0.92 %. The corresponding values of the modal mass, for the first mode, were found to be 0.066 kg and 0.17 kg (with modeshapes normalized such that  $\max[|\varphi_n(0 \leq x \leq L)|] = 1$ ). Notice that the added mass from the external fluid almost triples the modal mass of the tube. On the other hand, the viscous damping results obtained were found to be consistent with the semi-empirical formulation proposed by Rogers et al. [26].

Application of the general formulation (11) to our system has shown that the incidence of the fluid-elastic forces on the tube higher-order modes is negligible. Therefore, under flow conditions, the fluid-elastic coupling coefficients  $C_k(V_R)$  and  $C_d(V_R)$  are also easily inferred from the identified first modal frequency  $f_1(V_R)$  and damping value  $\zeta_1(V_R)$ , accounting for the added damping from the stabilizing feedback loop – see [12] for details.

The modal parameters, identified from the system response to the flow turbulence, are shown in Fig. 4 as a function of the flow velocity  $V$ . The fluid-elastic coefficients obtained are shown in Fig. 5 as a function of the reduced velocity  $V_R$ . Notice in Fig. 4 the increase in damping, and decrease in the modal frequency, when the stabilizing feedback loop is closed. In accordance with equation (9), the sign convention for the fluid-elastic coefficients plotted in Fig. 5 is such that positive values of  $C_k(V_R)$  would increase the modal frequency of the flow/structure coupled system. Similarly, positive values of

$C_d(V_R)$  are stabilizing. Notice that, for the full range of flow velocity explored in the tests,  $C_k(V_R)$  is negative, although its magnitude decreases as  $V_R$  increases. More importantly, as a general trend  $C_d(V_R)$  decreases as  $V_R$  increases, clearly becoming negative and leading to fluid-elastic instability beyond about  $V_R > 3.8$ . Also notice the sudden decrease of  $C_d$  near  $V_R \approx 2.2$ , a behavior which can be attributed to vortex shedding phenomena.

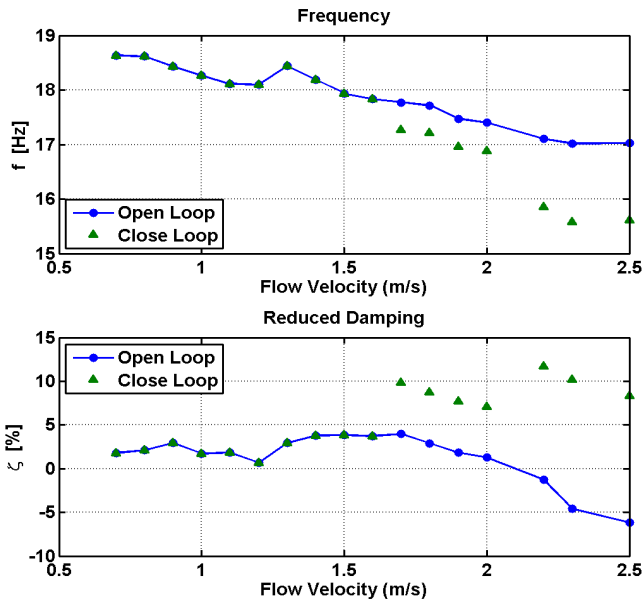


Figure 4: Identified modal frequency and damping of the first tube mode as a function of the flow reduced velocity (Open loop: stabilizing feedback off; Closed loop: stabilizing feedback on)

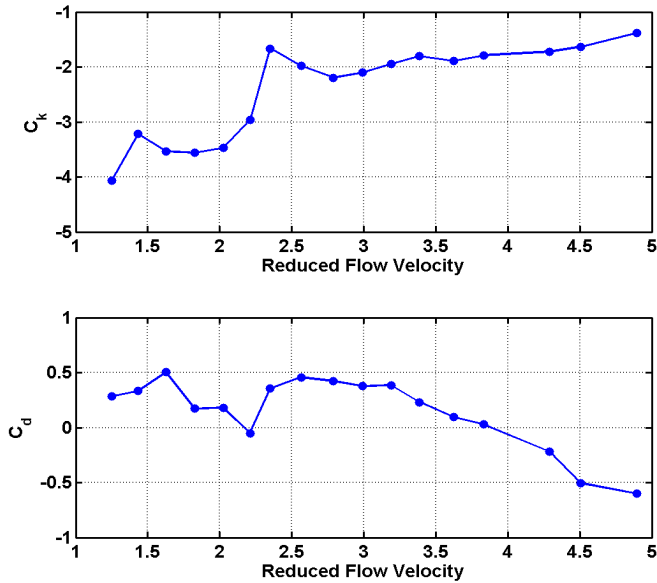


Figure 5: Identified dimensionless fluid-elastic coupling coefficients, as a function of the flow reduced velocity

## 4.2. Identified Turbulence Excitation

Using linear theory – see [19] for details – we identified the amplitude of the turbulence excitation spectrum from the vibratory response of the tube first mode, as the flow velocity was increased. The dimensionless results thus obtained are shown in Fig. 6, as a function of the reduced frequency  $f_r$ , and they are plotted superimposed with the reference spectrum  $[\Phi]_e(f_r)$  proposed as a design guideline by Axisa et al. [19]. One can notice that the agreement between the proposed reference spectrum and our experimental data is nearly perfect.

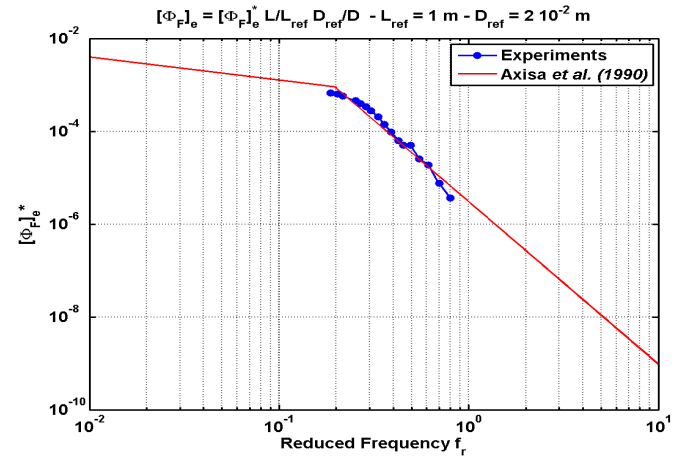


Figure 6: Identified excitation data, superimposed to the Equivalent Reference Spectrum of the turbulence forces per unit tube length proposed by Axisa et al. (1990)

## 5. COMPUTATIONAL AND EXPERIMENTAL LINEAR VIBRATORY RESPONSES

Before tackling the nonlinear part of this work, the linear experimental results have been confronted to our numerical simulation program, which was developed following the theoretical approach discussed in section 2. Figure 7 illustrates the first four modes shapes of the modal basis used in our numerical simulations, which were computed using a finite-element model. The modal frequencies and damping values used in the computations are those experimentally identified in still water. Notice that, because the tested tube is clamped to the wall through a flat bar, one should not expect the experimental modal frequencies to display the typical ratios of a common clamped-free tube.

The experimentally identified fluid-elastic coefficients are used in the computations. First, the tube response frequency  $\bar{f}_r(t)$  is estimated at each time step according to (18)-(19), from which the reduced velocity  $V_R(t)$  is computed, which enables the interpolation of  $C_k(V_R)$  and  $C_d(V_R)$  from the experimental data of Fig. 5. Concerning turbulence excitation, the perfect agreement between our experimental data and the excitation spectrum proposed by Axisa et al. [19] enable us to use the spectrum of Fig. 6 in total confidence.

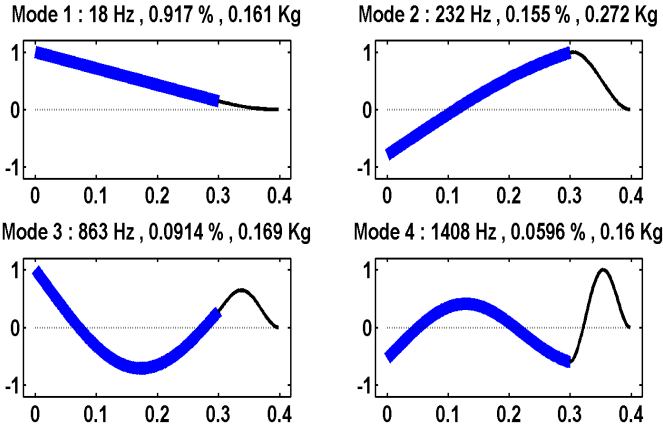


Figure 7: First modes of the modal basis used in the time-domain numerical simulations

Figure 8 presents a comparison between the measured modal frequency  $f_1$  and damping  $\zeta_1$  of the tube, as a function of the flow velocity, which are superimposed with those stemming from the eigen-formulation (11), where the experimentally identified coupling coefficients of Fig. 5 have been replaced. The perfect agreement demonstrates the overall coherence of the identification procedures and results.

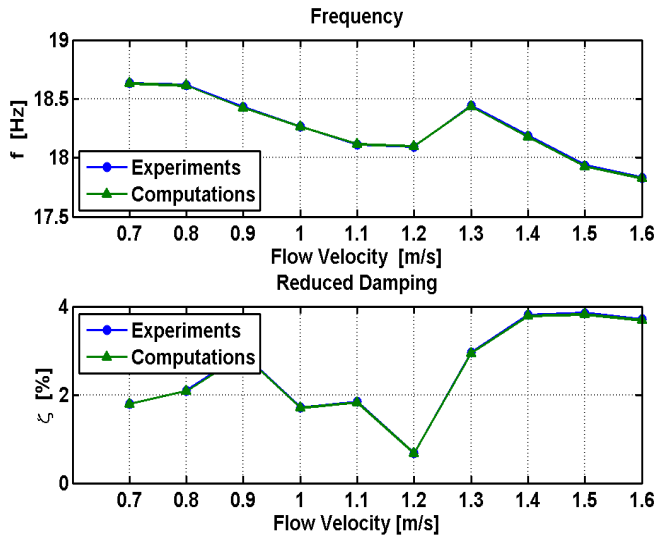


Figure 8: Comparison between the measured modal parameters and those computed from the identified fluid-elastic coefficients

## 6. COMPUTATIONAL AND EXPERIMENTAL VIBRO-IMPACT RESPONSES

### 6.1. Detailed Experimental and Computed Responses

We now address the final and most important aspect of this work, namely, asserting if the fluid-elastic coefficients obtained under steady oscillatory conditions may be used with confidence when modeling the unsteady nonlinear dynamics of

vibro-impacting flow-excited tubes. First, we illustrate the results obtained by showing detailed plots from experiments and computations at two different velocities and two values of the support gap. Then we present overall statistical results, for the complete range of velocity explored, comparing the experimental and computed vibro-impact forces and the tube response frequencies.

Figure 9 displays samples of the experimental and computed tube responses, for the flow velocity  $V = 2.1$  m/s with support gap  $\delta_c = \pm 0.5$  mm. Figure 10 presents the results obtained for  $V = 3.6$  m/s with  $\delta_c = \pm 1$  mm. In these figures are shown plots of the impact force at  $x_c$ , the tube displacement response at the free end of the tube, the corresponding response spectrum and amplitude histogram. Notice that the vibration amplitude is bounded at about the double of the gap  $\delta_c$  at location  $L/2$ , as can be understood from the first modeshape in Fig. 7.

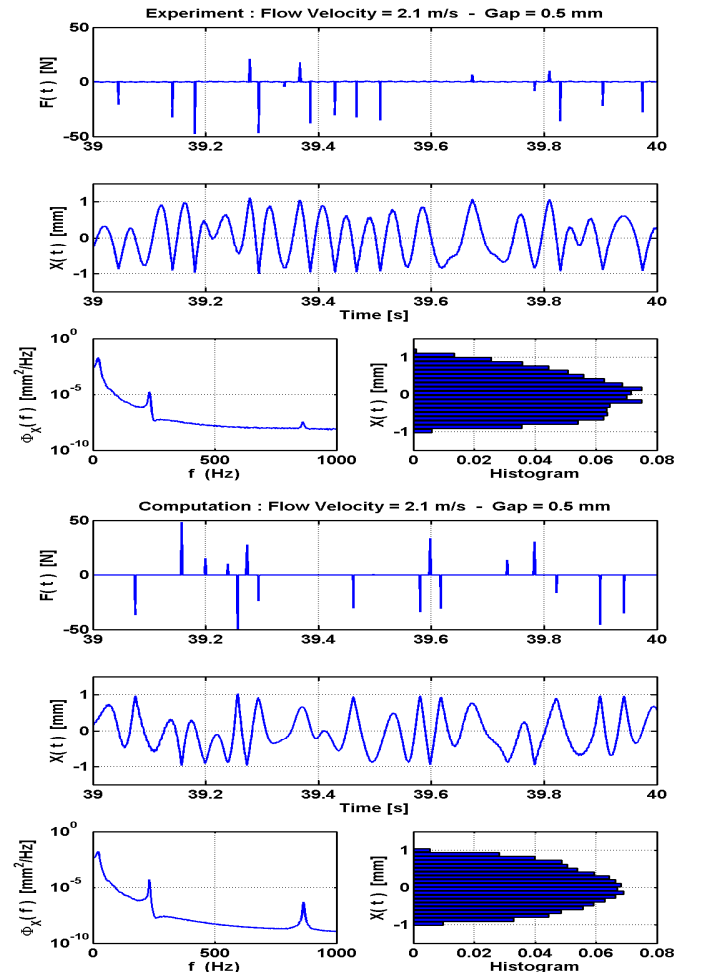
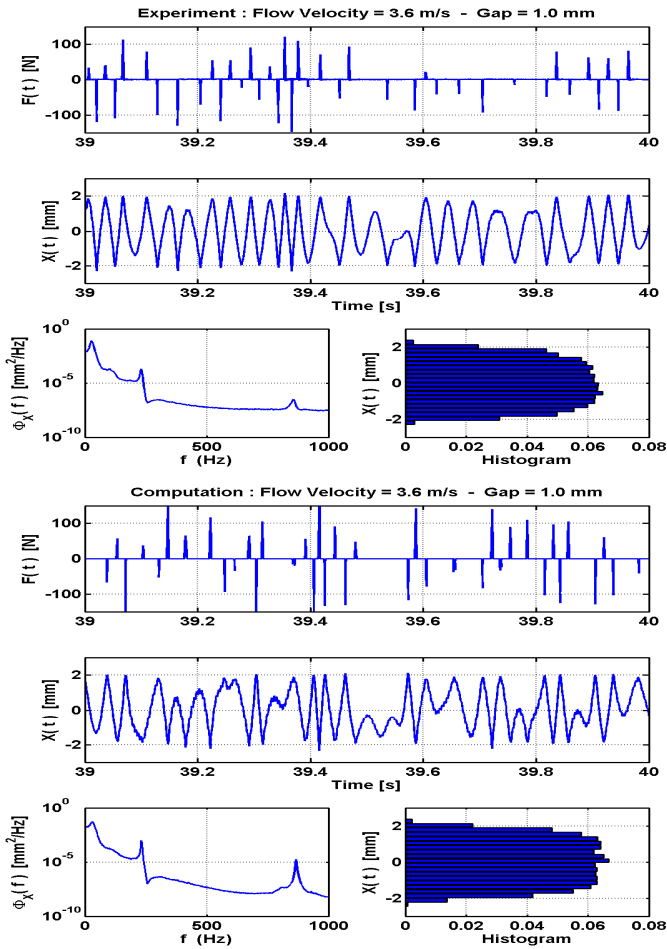


Figure 9: Comparison between the measured computed responses at velocity  $V = 2.1$  m/s with a support gap  $\delta_c = \pm 0.5$  mm

The results shown in Fig. 9, at velocity  $V = 2.1$  m/s ( $V_R = 3.4$ ), almost at the verge of fluid-elastic instability. The support gap  $\delta_c = \pm 0.5$  mm is small enough for relatively intense impacting, as a result of the turbulence forces. Notice the good agreement between all features of the experimental and computed responses, the sole differences concerning the higher-order modal spectral responses, which appear more damped in the experiments.



**Figure 10: Comparison between the measured and computed responses at velocity  $V = 3.6$  m/s with a support gap  $\delta_c = \pm 1$  mm**

Results in Fig. 10 concern the higher velocity  $V = 3.6$  m/s, which induces a severe fluid-elastically unstable system, using the larger support gap  $\delta_c = \pm 1$  mm. A violently nonlinear vibro-impacting regime is now obtained, with a far-from-Gaussian tube response. This is due in part to the higher turbulence excitation, but mostly to the large unstabilizing fluid-elastic coupling forces which, being proportional to the vibration amplitude, are enhanced by the larger support gap. Notice that, as before, the agreement between experiments and computations is very satisfying.

## 6.2. Global Results and Energy Aspects

The method developed here for the estimation of the computational response frequency could not be used on the experimental results, because not all the response signals  $Y(t)$ ,  $\dot{Y}(t)$  and  $\ddot{Y}(t)$  – used in equation (18) – were available in our measurements. Obviously, from the measured displacement, the velocity and acceleration could be derived, but at the cost of some noise amplification. We decided this was a good reason to compare the response frequencies  $\bar{f}_r$  predicted by our algorithm with a different method better suited to deal with the experimental results. Figure 11 shows the results obtained for the average response frequency, by processing the total length of the computed responses with Rice's formula and with our equivalent 1-dof oscillator method. It appears that, except at the lowest flow velocities when the system is stable, both methods produce similar results, for all practical purposes.

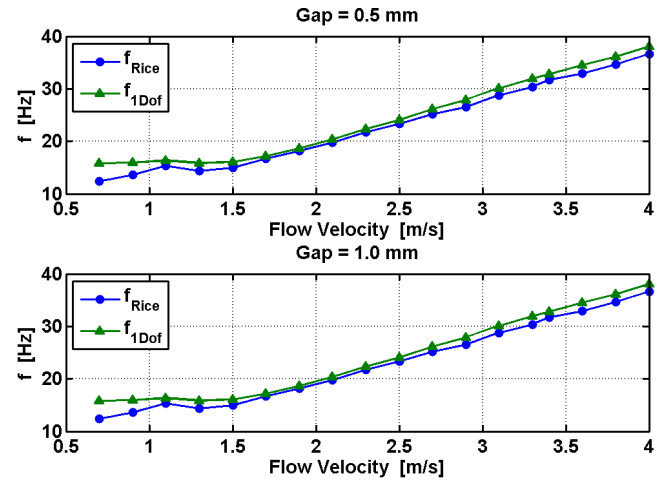


**Figure 11: Comparison between the response frequencies estimated using Rice's formula and the equivalent 1-dof oscillator technique**

In Figs. 12 and 13 we present a comparison between the experimental and computational results, for the complete range of flow velocity explored, and for the two support gaps tested. Figure 12 shows a quantifier (among other possible options) of the impact force magnitude – the average of the impact force maxima. For  $\delta_c = \pm 0.5$  mm, no impacts are displayed by the stable system up to  $V \approx 1$  m/s, this velocity being increased to  $V \approx 1.5$  m/s for the larger gap  $\delta_c = \pm 1$  mm. Then, the impact forces magnitudes increase steadily with the flow velocity. All qualitative features of the experimental results are perfectly reproduced by the computations, including the velocity boundaries where the tube starts to impact. Quantitatively, one may notice that the computed impact forces at higher flow velocities are about 20 % higher than the corresponding experimental forces. This difference might be due to the fact that in the computations we have neglected the impact damping

at the loose support. This aspect deserves to be further investigated.

An interesting point concerns the effect of the support gap on the magnitude of the impact forces. While the system is stable, because of the low vibratory amplitudes, higher forces are displayed by the smaller-gap system. However, as soon as the system becomes linearly unstable, higher impact forces are observed on the larger-gap system. This is simply because the fluid-elastic forces are proportional to the system vibratory amplitude and hence, beyond instability, increase almost proportionally with  $\delta_c$ .

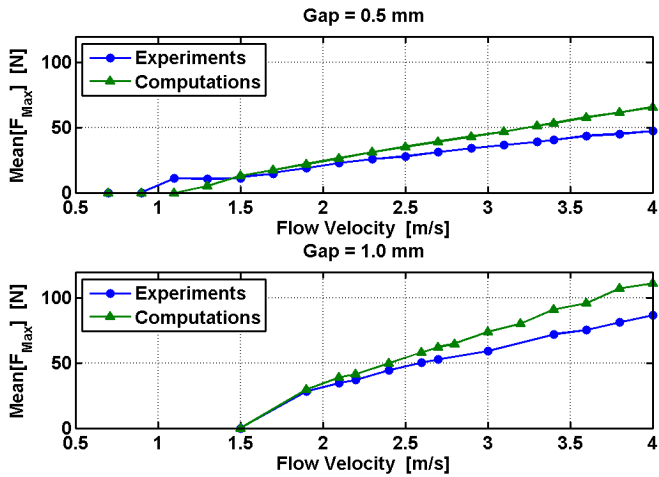


Figure 12: Comparison between the tube experimental and computed impact forces

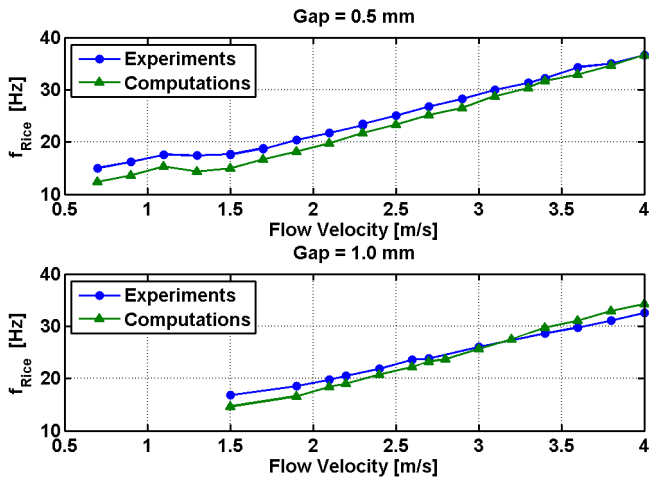


Figure 13: Comparison between the tube experimental and computed response frequencies

In Fig. 13 we present the experimental and computational response frequencies of the system (both estimated according to Rice's formula) and, again, their comparison is highly satisfactory. At low velocities, when the system is not impacting, the time-domain frequency responses are those of

the flow-coupled first mode. Then, beyond the instability boundary, the system experiences a steady increase of  $\bar{f}_{Rice}$  with the flow velocity. This result is a direct consequence of an increase in the system effective stiffness, connected with increasingly intense vibro-impact dynamical regimes.

The quite good agreement between the nonlinear experimental and computational results shown in Figs. 12 and 13 enable us to conclude that, in spite of having obtained the fluid-elastic coefficients  $C_k(V_R)$  and  $C_d(V_R)$  under steady oscillatory conditions, it is totally satisfactory to use them for performing severely nonlinear unsteady computations.

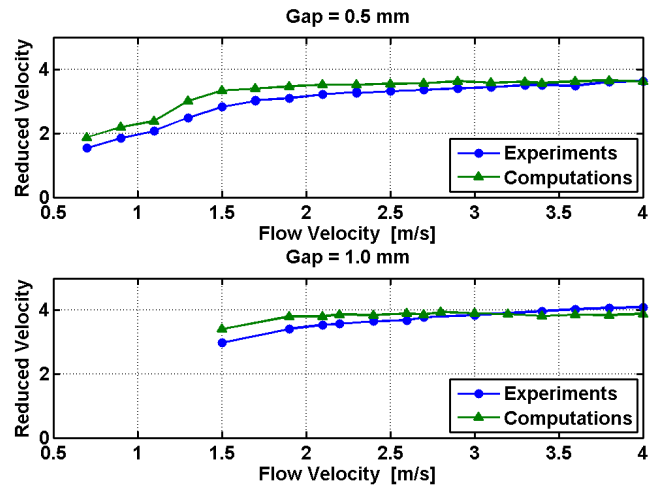


Figure 14: Comparison between the tube experimental and computed average reduced velocities as a function of the flow velocity

In Fig. 14 the average values of the reduced velocities obtained from the nonlinear experiments and computations are plotted as a function of the flow velocity. Recall that  $V_R$  only increases proportionally to  $V$  under linear conditions. For vibro-impacting systems their relationship is not straightforward, because the actual response frequency  $\bar{f}_r$  used in  $V_R = V/\bar{f}_r D$  is not constant, being dependent on the (a priori unknown) response regime of the nonlinear system. Having this in mind, the dynamical behavior of gap-supported tubes subjected to fluid-elastic forces is well clarified by Fig. 14. It appears that, beyond the linear instability boundary – and at least for a large range of flow velocity – the system dynamics self-regulate in order to produce a mean response frequency which leads to an almost-constant value of the reduced velocity.

The meaning of this is partly clarified by noting that the “asymptotic” value  $V_R^* \approx 4$  in the plots of Fig. 14 is the reduced velocity at which the coupling coefficient  $C_d(V_R)$  changes from positive to negative, see Fig. 5. Therefore, for a given flow velocity  $V > V_{crit}$ , the linearly unstable vibro-

impacting system will increase its response frequency up to a value  $\bar{f}_r^*$  such that  $C_d(V_R^*) \approx 0$ . This is the simple condition which enables a viable energy balance for this system, in which instability is controlled by damping. For flexible tube bundles, which may become unstable through damping and stiffness mechanisms, the conditions which define the nonlinear response regimes “chosen” by the system are possibly more involved. However, the same principle applies.

As a side point notice that, because the vibro-impacting system never “allows” average reduced velocities higher than  $V_R^* \approx 4$ , we may achieve credible nonlinear computations at flow velocities higher than those where the fluid-elastic coefficients of the linear system were identified.

The general discussion of Fig. 14 neglects the important role of the turbulence forces and will be now supplemented by the detailed information provided by the plots in Fig. 15. These were computed from the results of the numerical simulations, and quantify the energy “paths” in the system, for increasing values of the flow velocity and for the two support gaps addressed. Positive values indicate that energy is supplied to the tube, while negative values indicate dissipated energy. As expected, turbulence forces always supply energy and the structural damping is always dissipative.

The most interesting part in these plots relates to the energy behavior stemming from the fluid-elastic coupling terms. For the smaller gap system, it appears that the fluid-elastic forces associated with the nonlinear vibro-impact regime are of dissipative nature, irrespectively of the flow velocity. In other words, the “active” vibration source is the flow turbulence. However, for the larger-gap system, the scenario is quite different, because at higher velocities the fluid-elastic forces stemming from the nonlinear regime are destabilizing. In this case, the energy input is shared by both the turbulence and the fluid-elastic forces.

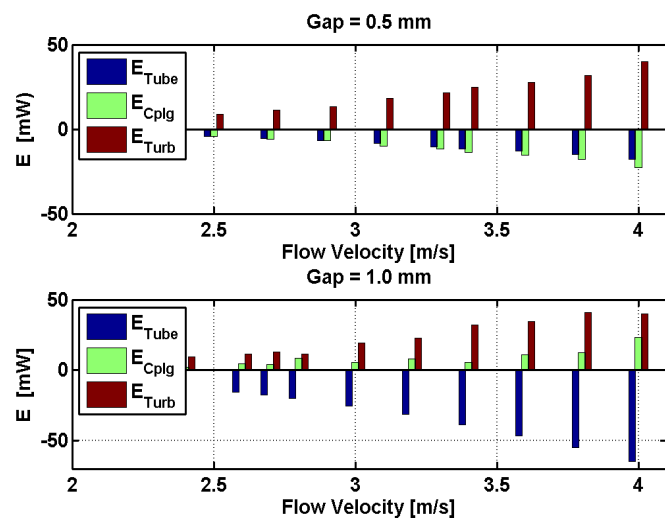


Figure 15: Computed energy terms as a function of the flow velocity and support gap

## 7. CONCLUSIONS

In this paper we presented experimental and computational results which constitute an overall validation of our approach to deal with gap-supported tubes subjected to fluid-elastic forces and flow turbulence excitation. The main point addressed was to assert the validity of computing the nonlinear and unsteady vibro-impact responses of fluid-elastically unstable tubes, knowing that the fluid-elastic coupling coefficients are typically provided by tests performed under steady oscillatory conditions.

The results obtained clearly demonstrate that such modeling approach is consistent with the nonlinear experiments, and therefore reliable. Because our general modeling framework is shared by other researchers, they may also feel reassured by the present investigation.

Among other aspects developed in this work, several techniques were reviewed for estimation of the “instantaneous” response frequency of nonlinear regimes. A new simple method, well suited for the nonlinear computations, was proposed and applied.

New experimental identifications of the fluid-elastic coefficients were performed, using a feedback stabilizing technique which allows for identifications at high flow velocities. Our experimental coefficients, obtained on a flexible tube within a rigid tube bundle with  $P/D = 1.5$ , corroborate those previously obtained [12]. On the other hand, we identified the turbulence excitation spectrum for our test rig, obtaining results which lay perfectly on the reference spectrum recommended by Axisa et al. [19].

Finally, under nonlinear conditions, extensive experiments and computations were performed, for a large range of flow velocity and two values of the tube support gap. Beyond providing a global validation of our modeling approach, the results obtained offer interesting insights on the nonlinear behavior of the tube. In particular, it became clear how the average response frequency is established by the vibro-impacting system. On the other hand, the analysis of the results provided by the two support gaps tested highlight possible scenarios which may arise, with respect to the various terms involved in an energy balance of the flow-excited tube.

## ACKNOWLEDGMENTS

The authors acknowledge financial support for this work, which was performed in the framework of a joint research program co-funded by AREVA NP, EDF and CEA (France). Also, concerning the experimental part of this paper, we gladly acknowledge the valuable contribution of THIERRY VALIN, from CEA/DEN/DM2S/SEMT/DYN (Saclay, France).

## REFERENCES

- [1] Tanaka H., Takahara S. (1981), “Fluidelastic Vibration of Tube Arrays in Cross-Flow”, *Journal of Sound and Vibration*, Vol. 77, pp. 19-37.
- [2] Connors H.J. (1970), “Fluidelastic Vibration of Tube Arrays Excited by Cross-Flow”, *Proc. Flow-Induced*

- Vibration in Heat-Exchangers* (Reiff, D.D. Ed), ASME, pp. 42-46.
- [3] Axisa F., Antunes J., Villard B. (1988), "Overview of Numerical Methods for Predicting Flow-Induced Vibration", *ASME Journal of Pressure Vessel Technology*, Vol. 110, pp. 6-14.
- [4] Fricker A. (1992), "Numerical analysis of the fluid-elastic vibration of a steam generator tube with loose support", *Journal of Fluids and Structures*, Vol. 6, pp. 85-107.
- [5] Rao M.S., Steinger D.A., Ahluwalia, K.S., Eisinger F.L. (1992), "Simulation of PWR Steam Generator Tubes Undergoing Turbulence and Fluidelastic Excitation for Wear Prediction", *ASME International Symposium on Flow-Induced Vibrations and Noise*, Anaheim, USA, Vol. 230, pp. 185-210.
- [6] Sauvé R.G. (1996), "A Computational Time Domain Approach to Fluidelastic Instability for Nonlinear Tube Dynamics", *Symposium on Flow-Induced Vibrations*, Montreal, Canada, ASME PVP/ICPVT-8, pp. 111-121.
- [7] Hadj-Sadok C., Payen T., De Langre E. (1997), "Modelling of Fluidelastic Vibrations of Heat Exchanger Tubes with Loose Supports", *4<sup>th</sup> International Symposium on Fluid-Structure Interaction, Aeroelasticity and Flow-Induced Vibration and Noise*, 16-21 November 1997, Dallas, USA, Vol. 53-2, pp. 193-199.
- [8] Hassan M., Hayder M. (2008), "Nonlinear Vibrations of Loosely Supported Tubes Excited by Fluidelastic and Turbulence Forces", *Nuclear Engineering and Design*, Vol. 238, pp. 2507-2520.
- [9] Antunes J., Axisa F., Vento M.A. (1992), "Experiments on Tube-Support Interaction with Feedback Controlled Instability", *ASME Journal of Pressure Vessel Technology*, Vol. 114, pp. 23-32, 1992.
- [10] Vento M.A., Antunes J., Axisa F. (1992), "Tube/Support Interaction Under Simulated Fluidelastic Instability: Two-Dimensional Experiments and Computations of the Nonlinear Responses of a Straight Tube", *Symposium on Flow-Induced Vibration and Noise*, Anaheim, USA, ASME PVP-242, pp. 151-166.
- [11] Mureithi N., Ito T., Nakamura T. (1996), "Identification of Fluidelastic Instability Under Conditions of Turbulence and Nonlinear Tube Supports", *ASME Pressure Vessel and Piping Conference, Montreal, Canada*, ASME PVP-328, pp. 19-24.
- [12] Caillaud S., De Langre E., Piteau P. (1999), "The Measurement of Fluidelastic Effects at Low Reduced Velocities Using Piezoelectric Actuators", *ASME Journal of Pressure Vessel Technology*, Vol. 121, pp. 232-238.
- [13] Caillaud S., De Langre E., Piteau P. (2000), "Measurement of Critical Velocities for Fluidelastic Instability Using Vibration Control", *ASME Journal of Vibration and Acoustics*, Vol. 122, pp. 341-345.
- [14] Caillaud S., De Langre E., Baj F. (2003), "Active Vibration Control for the Measurement of Fluidelastic Effects", *ASME Journal of Pressure Vessel Technology*, Vol. 125, pp. 165-170.
- [15] De Araujo M., Antunes J., Piteau P. (1998), "Remote Identification of Impact Forces on Loosely Supported Tubes : Part 1 — Basic Theory and Experiments", *Journal of Sound and Vibration*, Vol. 215, pp. 1015-1041.
- [16] Antunes J., Axisa F., Beaufile B., Guilbaud D. (1990), "Coulomb Friction Modelling in Numerical Simulations of Vibration and Wear Work Rate of Multi-Span Heat-Exchangers", *Journal of Fluids and Structures*, Vol. 4, pp. 287-304.
- [17] Lever J.H., Weaver D.S. (1982), "A Theoretical Model for the Fluidelastic Instability in Heat Exchanger Tube Bundles", *ASME Journal of Pressure Vessel Technology*, Vol. 104, pp. 147-158.
- [18] Granger S., Campistron R., Lebre J. (1993), "Motion-Dependent Excitation Mechanisms in a Square In-Line Tube Bundle Subject to Water Cross-Flow: An Experimental Modal Analysis", *Journal of Fluids and Structures*, Vol. 7, pp. 521-550.
- [19] Axisa F., Antunes J., Villard B. (1990), "Random Excitation of Heat-Exchanger Tubes by Cross-Flow", *Journal of Fluids and Structures*, Vol. 4, pp. 321-341.
- [20] Antunes J., Delaune X., Piteau P., Borsoi L. (2008), "A Simple Consistent Method for the Time-Domain Simulation of Turbulence Excitations Applied to Tube/Support Dynamical Analysis Under Non-Uniform Flows", *9<sup>th</sup> International Conference on Flow Induced Vibrations (FIV-2008)*, 30 June-3 July 2008, Prague, Czech Republic.
- [21] Antunes J., Piteau P., Delaune X., Borsoi L. (2009), "An Evaluation of Methods for the Time-Domain Simulation of Turbulence Excitations for Tube Bundles Subjected to Non-Uniform Flows", *20<sup>th</sup> International Conference on Structural Mechanics in Reactor Technology (SMIRT 20)*, 9-14 August 2009, Espoo, Finland.
- [22] Rice S.O. (1945), "Mathematical Analysis of Random Noise", *Bell System Technical Journal*, Vol. 24, pp. 46-156.
- [23] Au-Yang M.K. (2002), "The Crossing Frequency as a Measure of Heat Exchanger Support-Plate Effectiveness", *Journal of Fluids and Structures*, Vol. 16, pp. 83-92.
- [24] Boashash B. (1992), "Estimating and Interpreting the Instantaneous Frequency of a Signal – Part 1: Fundamentals; Part 2: Algorithms and Applications", *Proceedings of IEEE*, Vol. 80, pp. 519–568.
- [25] Pachet F., Briot J.P. (Eds.) (2004), " Informatique Musicale: Du Signal au Signe Musical" (Chapter 1), *Hermès Science Publications*, Paris, France.

[26] Hart G.C., Wong K. (1999), "Structural Dynamics for Structural Engineers", *John Wiley & Sons*, New York, USA.

[27] Rogers R.J., Taylor C., Pettigrew M.J. (1984), "Fluid Effects on Multispan Heat-Exchanger Tube Vibration", *ASME Pressure Vessel and Piping Conference*, San Antonio, USA.